Physics – Uspekhi **61** (10) 1000 – 1015 (2018)

FROM THE CURRENT LITERATURE

PACS numbers: 61.50.ks, 61.66.Dk, 64.70.K–

Some discussion topics on the representation of the equilibrium Fe – Ni phase diagram and on the nature of the Invar effect

N D Zemtsova

DOI: https://doi.org/10.3367/UFNe.2018.02.038298

Contents

Abstract. This paper presents a thorough analysis of Fe – Ni phase diagrams published over the last 50 years. It is shown that the differences in drawing the low-temperature part of the phase diagram and in the explanation of the nature of Invar alloys are due to a lack of clear experimental evidence for the absence or occurrence of a particular superstructure in the range of compositions with less than 50% Ni content. The experimental results obtained favor a certain particular phase diagram as yet unpublished in the reference literature, and suggest the possible origin of the Invar effect. The phase diagram analysis and the assumption on the nature of the Invar effect are based on results obtained by structural methods.

Keywords: Fe – Ni diagram, Invar effect, microdomains, discontinuous coagulation, discontinuous decomposition, reverse $\alpha \rightarrow \gamma$ transformation

1. Introduction

Alloys of the Fe – Ni system constitute the basis of many technologically important industrial materials. Understanding the patterns of formation of their physical properties is necessary in order to solve many metals-science problems.

Results of investigations of phase and structural transformations in the alloys of this system are presented in many studies. The first publications of the Fe – Ni phase diagram [1] date to the 1920s. Currently, however, not only is a unified opinion on the position of the phase boundaries in the region of low temperatures absent, but even the very presence of different ordered phases in the relevant diagram is questioned.

N D Zemtsova Mikheev Institute of Metal Physics,
Ural Branch of the Russian Academy of Sciences,
ul. S Kovalevskoi 18, 620990 Ekaterinburg, Russian Federation
E-mail: zemtsova@imp.uran.ru

Received 4 July 2017
Uspekhi Fizicheskikh Nauk **188** (10) 1103 – 1118 (2018)
DOI: https://doi.org/10.3367/UFNr.2018.02.038298
Translated by S N Gorin; edited by A Radzig

The difficulty of obtaining reliable results on the precise position of the boundaries of phase fields is due to the extreme slowness of diffusion processes and the close values of the self-diffusion coefficients of iron and nickel atoms at temperatures below 600 °C. To increase the rate of the formation of an ordered state of phases, the alloys were irradiated in a number of studies [2–6] by electrons with an energy from 1 to 5 MeV, which leads to the appearance of radiation defects in the crystal structure: vacancies and interstitial atoms, which substantially increase the diffusion mobility of iron and nickel atoms, thereby facilitating the approach of the alloy structure to an equilibrium state in the annealing process.

Together with the above method, some other methods were applied to prepare properly alloy samples; in particular, in Ref. [4] a study was carried out of an Fe–49.5 wt.% Ni sample prepared by the deposition of the alloy vapors onto a carbon substrate at room temperature. In the samples of the alloys prepared by this method, a high concentration of excess vacancies appears. The subsequent annealing of the disordered samples prepared by these two methods led to the realization of identical phase compositions. This experiment confirms that the excess vacancies created upon electron beam irradiation facilitate the ordering reaction, accelerating its kinetics, but do not induce it. Therefore, we will analyze in this article in equal degree the experimental results obtained both on irradiated and on unirradiated samples in the annealing process.

In this article, we will not consider phase diagrams published more than a half-century ago. We concentrate our attention mainly on the diagrams published in recent years, including those found in the reference literature.

In the phase diagram given in book [7] with reference to paper [8], three ordered phases are present. The critical transition temperatures of ordering these phases grow with an increase in the content of nickel (Fig. 1). These ordered phases are also present in the diagram given in Kubaschewski's handbook [9] with reference to paper [2] (Fig. 2a). The critical ordering temperatures T_{cr} of Fe_3Ni and FeNi phases are tagged by the question mark, which reflects contradictions in the presentation of this phase diagram by

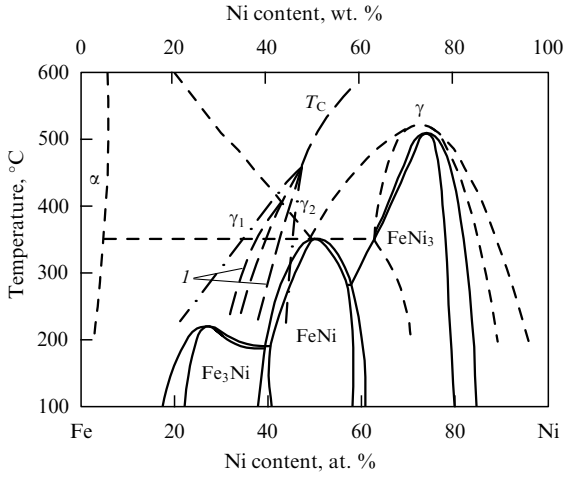

Figure 1. Generalized phase diagram of the Fe–Ni system: (*1*) curves of spinodal decomposition. (The diagram is taken from Ref. [7] and was first published in paper [8].)

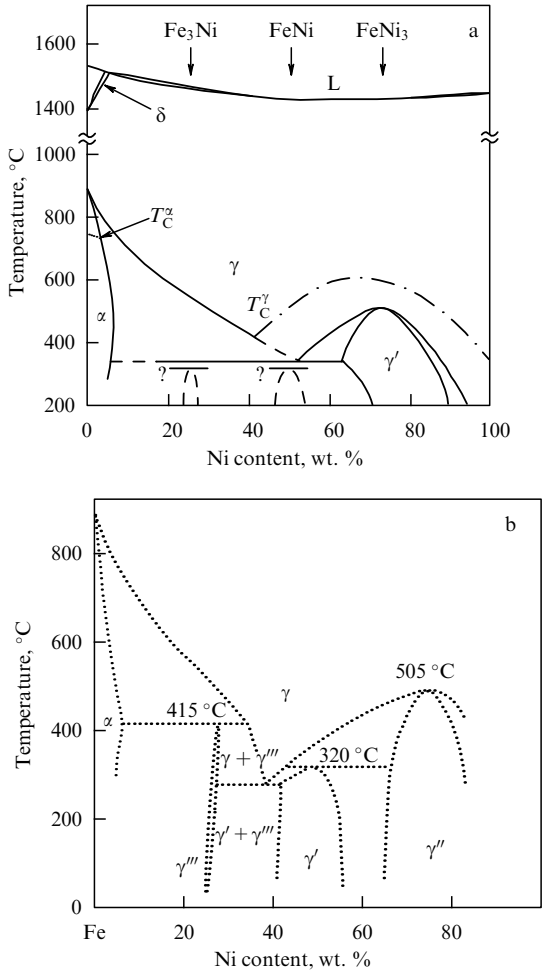

Figure 2. (a) Fe–Ni phase diagram published in Ref. [9] with the reference to paper [2]. (b) Fe–Ni phase diagram borrowed from paper [2].

different authors, and also the absence of reliable experimental proof of the stability of these phases and fields of their existence. These phases are called in handbook [9] hypothetical. However, it should be noted that in paper [2] there is a diagram (Fig. 2b) with a sufficiently clear indication of the T_{cr}

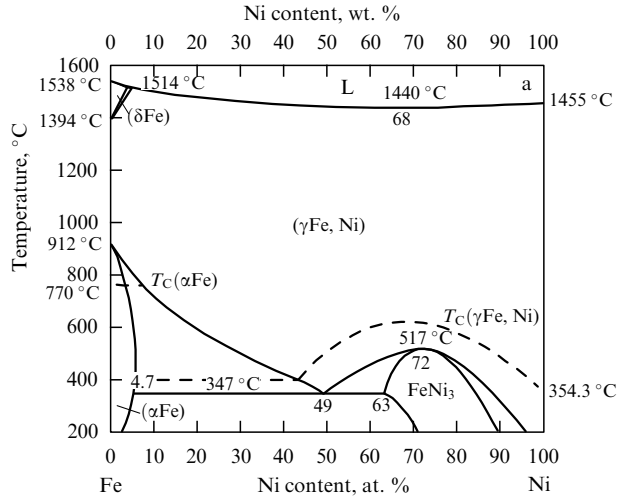

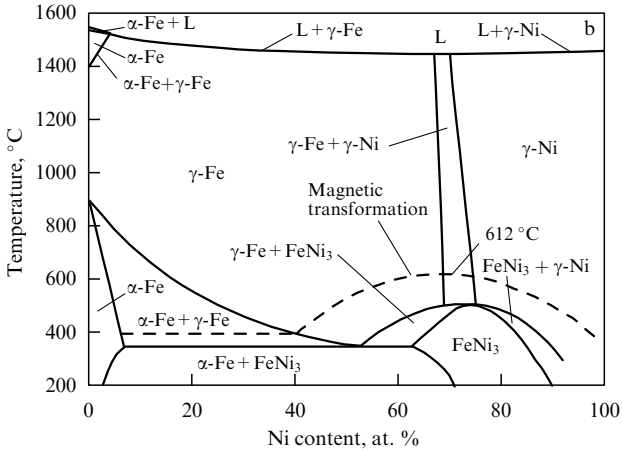

Figure 3. Fe–Ni phase diagrams published (a) in [7] and (b) in [10]. In the region of low temperatures, these diagrams are identical.

values for the Fe_3Ni and FeNi compositions. Moreover, the values of T_{cr} decrease with an increase in the content of nickel, in contrast to the values of T_{cr} given in Fig. 1 [7]. Notice that in the same reference book [7] there is one more phase diagram (Fig. 3a), in which these ordered phases are completely absent. No discrepancies exist only relative to the presence of the ordered $FeNi_3$ phase in the region of compositions with an enhanced content of nickel.

Reference [10] plots a compilation diagram (see Fig. 3b), in which the phases Fe_3Ni and FeNi are also absent. The last diagram in the low-temperature region coincides at all compositions with the diagram presented in Fig. 3a. These diagrams were constructed mainly on the basis of the results of an investigation of phase equilibria in high-purity alloys synthesized by the deposition of iron and nickel vapors onto a substrate [11]. It has been shown by the X-ray diffraction method that at a temperature of 345 °C an eutectoid equilibrium $\alpha + FeNi_3$ is established. On this basis, the authors of Refs [10, 11] suggest that the low-temperature region of the Fe–Ni phase diagram be considered the region of the co-existence of equilibrium phases α and $FeNi_3$, where α is a body-centered cubic (bcc) phase with an Ni content of 4.9 at.%. The same conclusion was made by the authors of studies [3, 12] performed by the neutron diffraction method (with the aid of small-angle magnetic neutron scattering). The presence of smeared and poorly resolved superlattice reflec-

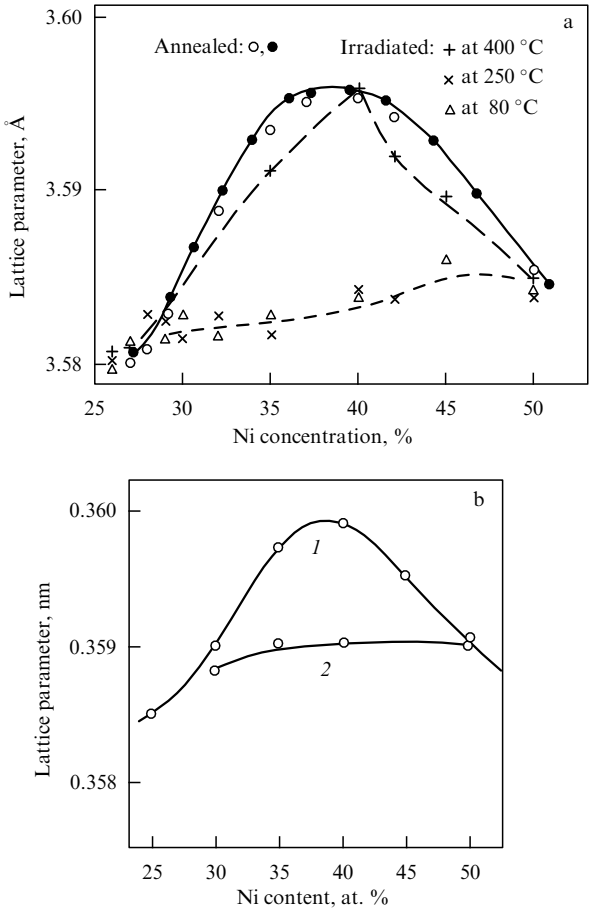

Figure 4. Lattice parameters measured at room temperature before and after electron irradiation, published (a) in Ref. [2] and (b) in Ref. [15]. The lattice parameters of alloys with a nickel content of 30–50% after irradiation are practically identical. The alloys used in Ref. [15] contained 0.01% carbon.

tions I_{100} and I_{110} in the neutron diffraction patterns of alloys with a nickel content of less than 40 at.% is considered to be the result of concentration disordering of the long-range order far from the stoichiometric composition $FeNi_3$.

In Refs [2, 13, 14], an assumption was made, based on a study of the intensity of diffuse nuclear neutron scattering in Fe–(30–35) at.% Ni alloys containing the ^{62}Ni isotope, on the possible formation of an Fe_3Ni superstructure. In paper [12], an experimental fact was demonstrated of an increase in the diffuse intensity of small-angle neutron scattering upon a decrease in the nickel content in alloys from 40 to 30%, which, in our opinion, correlates with the assumption proposed in Refs [2, 13, 14]. However, the authors of Refs [3, 12] reach a conclusion that the Fe_3Ni superstructure, assumed to be formed in Refs [13, 14], is not realized in Invar alloys [3].

The uncertainty in the determination of one ordered phase or another is because of the very close values of the lattice parameters for the Fe_3Ni, FeNi, and $FeNi_3$ phases. In Figs 4a and 4b, experimental values are given of the lattice parameters for phases that are formed in Fe–Ni alloys after irradiation by electrons and/or annealing. The difference in the crystal lattice parameters of possible phases with differing superlattices $L1_2$ and $L1_0$ is so small ($\Delta a = \pm 0.0003$ nm) that, even with an X-ray diffraction study, the superstructure reflections are superimposed on each other. This makes it difficult to determine which superstructure reflections concretely belong to a particular ordered phase [2, 4, 15].

To increase the intensity of superstructure reflections in the electron diffraction patterns of alloys with the nickel content of 30–50 wt.%, the authors of work [4] oriented the foils in an electron microscope in such a manner that only one systematic row of reflections, hh0 or 00h, turned out to be intense. This made it possible to convincingly show the very fact of the presence of the ordered phase in the entire investigated interval of the Fe–Ni alloy concentrations. But the authors of Ref. [4] did not reveal any difference in the interplanar spacings based on the analysis of superstructure reflections for all the alloys. Therefore, they suggested the formation of one phase with the $L1_0$ superstructure and an increase in the critical temperature T_{cr} from 260 °C for 30% Ni to 320 °C at 50% Ni. This conclusion was made by the authors of Ref. [4] based on the correspondence of the temperature $T_{cr} = 320$ °C determined in their work with that established in Ref. [16] for the equiatomic alloy and on the absence of such a correspondence with the results of paper [2], in which a higher value of T_{cr} was found for the alloy with 35 wt.% Ni compared with T_{cr} for the equiatomic alloy (Fig. 2b). The authors of study [2] ascribed this increase in T_{cr} to the formation of another phase, Fe_3Ni, ordered according to the $L1_2$ type.

The authors of Ref. [17] in their electron-microscopic study of the Fe–32.5% Ni alloy single crystals after their heating to the temperature of 470 °C for 1.5–2.0 h proved the formation of an ordered $L1_2$ phase based not only on the angles of the location of superstructure diffraction spots, but also on the orientations of planes of the face-centered cubic (fcc) lattice corresponding to the superstructure spots. The following conclusion was made: the composition of the phase comes after Fe_3Ni rather than $FeNi_3$. However, this conclusion was made by the authors of Ref. [17] based on the analogy with the Cu–Au system, in which the formation of two $L1_2$ superstructures was reliably established: Cu_3Au and Au_3Cu. Since in alloys close in composition to Ni_3Fe an ordered Ni_3Fe phase with a face-centered cubic lattice was found, the authors of Ref. [17] supposed that the formation of another Fe_3Ni superstructure can be expected with the availability of stoichiometric Fe_3Ni composition. The dissolution of 1.7% carbon in the Fe–32.5% Ni led to an increase in T_{cr}, an enhance in the lattice parameter of the ordered structure, and a strengthening of the intensity of superstructure spots.

In our opinion, the most reliable and simplest indicator of the presence of the Fe_3Ni phase is the occurrence of a central peak in the nuclear gamma-resonance (Mössbauer) spectra, which indicates the presence of a paramagnetic phase [2, 15]. In alloys with a composition close to Fe–25 at.% Ni, this peak is registered immediately after quenching the alloy from the austenitic region. In alloys far from this composition, the central peak is recorded after irradiation by electrons or by neutrons (see Fig. 5a [2] and Fig. 5b [15]).

However, in Refs [15, 20, 21] this evidence (reliable, in our opinion) of the formation of the paramagnetic Fe_3Ni phase is connected with the magnetic inhomogeneity of austenite, which appears in the initially ferromagnetic state of alloys with an Invar composition upon low-temperature annealing, deformation, or irradiation. However, this separation in composition into iron-depleted and iron-enriched regions cannot lead to the observed significant increase in the

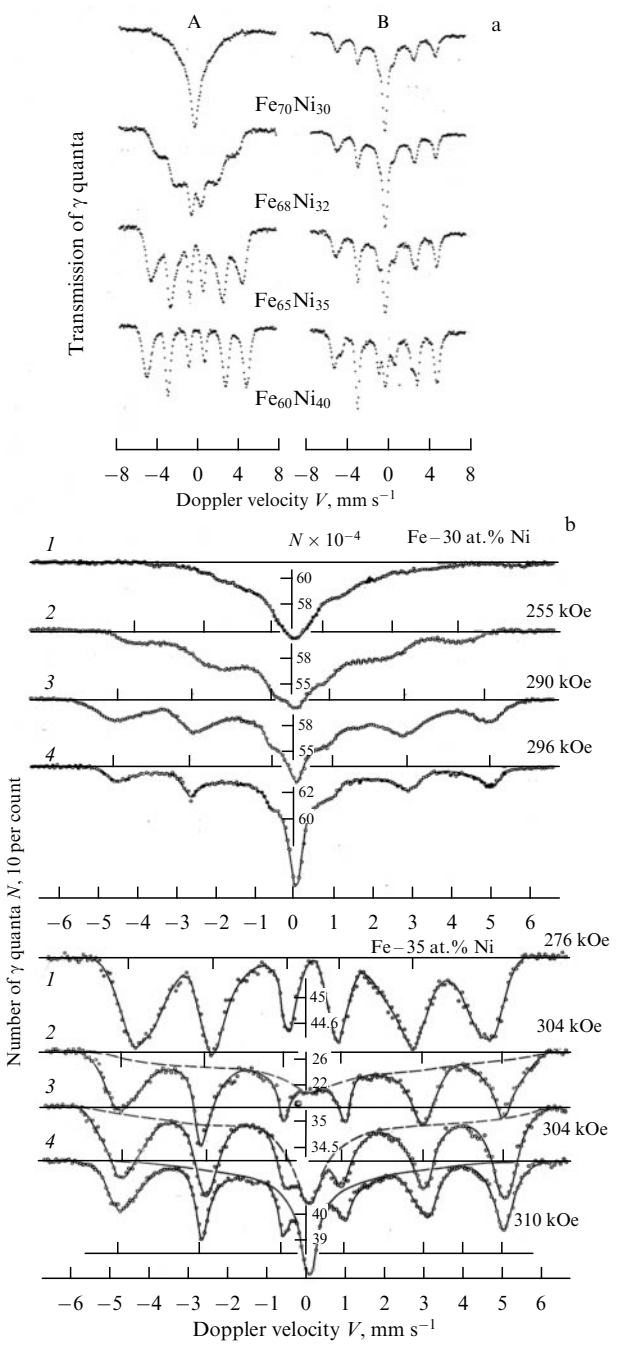

Figure 5. (a) Mössbauer spectra before (A) and after (B) irradiation by electrons. The composition of the alloys is indicated in the figure. (Taken from Ref. [2]). (b) Mössbauer spectra of Fe–30 at.% Ni and Fe–35 at.% Ni alloys after quenching from the temperature of 1100 °C (*1*) and after irradiation by electrons at doses of (*2*) 10^{18} cm^{-2}, (*3*) 10^{19} cm^{-2}, and (*4*) 5×10^{19} cm^{-2}. The value of the maximum magnetic field is indicated to the right of each spectrum.

strength properties of the alloy [22, 23], to a lowering in the temperature of the onset of the martensitic transformation, or even to a change in its kinetics [24]. A substantial increase in the resistivity cannot be explained by a phase separation of the initially homogeneous solid solution either, but agrees well with the model of the decomposition of an alloy into two phases [6]. A more significant change in the electrical resistance of the alloy enriched with phosphorus, which is an interstitial element, indirectly indicates that the precipitation of precisely an ordered phase occurs.

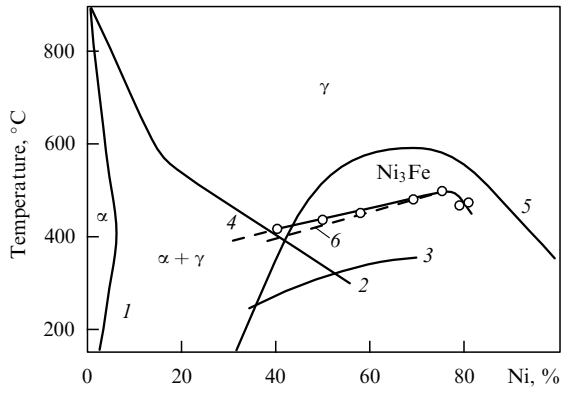

Figure 6. Fe–Ni phase diagram (reproduced from Ref. [3]): (*1*) boundary of the α/γ transition; (*2*) boundary of the γ/α transition; (*3*) boundary of the region of existence of the FeNi superstructure [$L1_0$]; (*4*) boundary of the region of existence of the Ni_3Fe long-range order [$L1_2$]; (*5*) Curie temperature, and (*6*) boundary of the two-phase order–disorder region.

The experimental facts presented in Refs [6, 17] are in agreement with the results of theoretical calculations [18, 19]: the presence of interstitial atoms of any kind increases the lattice parameter and the critical ordering temperature. Experimental confirmation of this for Fe–Ni alloys can be seen in Figs 4a and 4b: an enhanced value of the lattice parameter in Fig. 4b is due to the presence of carbon.

The presence or the absence of the central peak in the Mössbauer spectrum of the quenched alloy can also depend on the temperature and on the rate of quenching from the austenitic region, since at high temperatures the phase separation in Fe–Ni alloys was registered experimentally [25]. The quenching from reduced temperatures of austenization will lead to registering the central peak.

The presence of the $L1_0$ ordered FeNi phase in the phase diagram has not been established unambiguously either. In the diagram given in Ref. [3] (Fig. 6), this phase is shown, but it is located in the region of concentrations of the formation of the ordered phase $FeNi_3$ at a lower temperature. Possible mechanisms of the $FeNi_3 \rightarrow FeNi$ transformation with a decrease in the temperature are not discussed in Ref. [3]. In our opinion, such a representation of the Fe–Ni diagram is erroneous and, apparently, is caused precisely by the existence of two $L1_2$ ordered phases different in compositions — Fe_3Ni and $FeNi_3$ — on opposite sides of the $L1_0$-FeNi superstructure and by a small difference between the lattice parameters of their crystal structures.

Sufficiently convincing experimental proof of the realization of the $L1_0$ superstructure in alloys close to the equiatomic composition are presented in Ref. [16]: the neutron irradiation of single crystals of the Fe–50 wt.% Ni alloy in a magnetic field at temperatures of up to 320 °C leads to the creation of a texture of an ordered phase with the tetragonality axis [001] parallel to the direction of the magnetic field. This phase can be only $L1_0$-FeNi, since the formation of a texture in alloys with a face-centered cubic lattice of the $L1_2$ type is impossible.

In Ref. [4], an Fe–49.5 wt.% Ni alloy prepared by the deposition of iron and nickel vapors onto a substrate was studied. After annealing at a temperature of 200 °C, dispersed precipitates of a new phase are revealed with the aid of electron microscopy; in diffraction patterns, rings of superstructure reflections are clearly registered. Since the diffraction pattern consists of rings rather than of spots (the grain

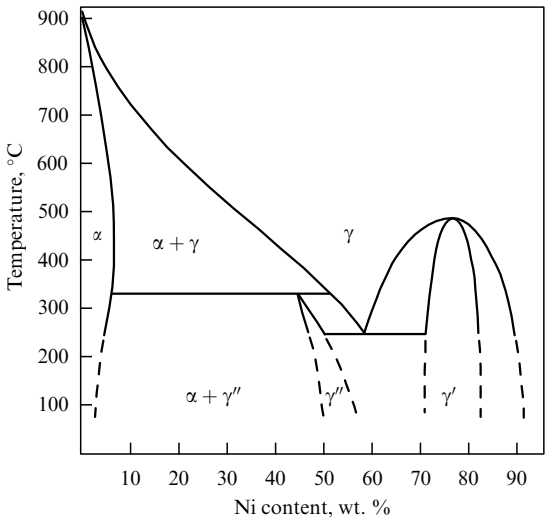

Figure 7. Fe – Ni phase diagram constructed on the basis of the analysis of the structure of a meteorite. (Taken from Ref. [26].)

size in the deposited samples is very small), the determination of the type of superstructure is sufficiently reliable: $L1_0$-FeNi. It has been established that the critical ordering temperature T_{cr} for the FeNi alloy is 320 °C, and this superstructure must be present in the phase diagram. Another indication in favor of the realization of the $L1_0$ superstructure is the quadrupole splitting of Mössbauer peaks noted in work [15].

In Ref. [3], the prolonged annealing of alloys with an Ni content of 45 and 55% were carried out at higher temperatures: 400 – 600 °C; it is for this reason that an ordered state was not obtained.

The authors of Refs [4, 5, 26–29] believe that the structural state closest to equilibrium is formed in meteorites, since the rate of their cooling is 1 °C in 10^6 years [26, 29]. Therefore, the structure of meteorites can serve as a standard for the presence of various equilibrium phases in the phase diagram of Fe – Ni alloys at low temperatures. In Ref. [26], the presence of an $L1_0$ structure of FeNi in meteorites was reliably established, and the phase diagram with the presence of this phase is given (Fig. 7). The lattice parameters of the FeNi-γ'' phase were found to be as follows:

$$a = (3.5761 \pm 0.0005)\ \text{Å}\,, \quad c = (3.5890 \pm 0.0005)\ \text{Å}\,,$$

$$\frac{c}{a} = (1.0036 \pm 0.0002)\,.$$

No Fe_3Ni phase with the $L1_2$ structure was revealed.

The analysis of the structure of meteorites in Refs [4, 28] showed the presence of both ordered phases: FeNi and Fe_3Ni (Fig. 8a), but in the phase diagram presented in Ref. [28], the Fe_3Ni phase was absent. Without explanation, the authors assumed this phase to be metastable. Later, in Ref. [29], a new, corrected, Fe – Ni diagram was presented (Fig. 8b), in which the $L1_0$-FeNi phase was also excluded from the stable phases. This correction was based on the results of the thermodynamic calculations carried out in Refs [21, 22], which took into account the magnetic effect on the Gibbs free energy. The sharp dependence of the Curie temperature on the composition of the alloy (dashed–dotted curve in Fig. 8b) changes the stability of phase equilibria. As a result, both phases, $L1_0$-γ''(FeNi) and $L1_2$-γ'''(Fe_3Ni), turn out to be metastable. On this basis, the following conclusion is made

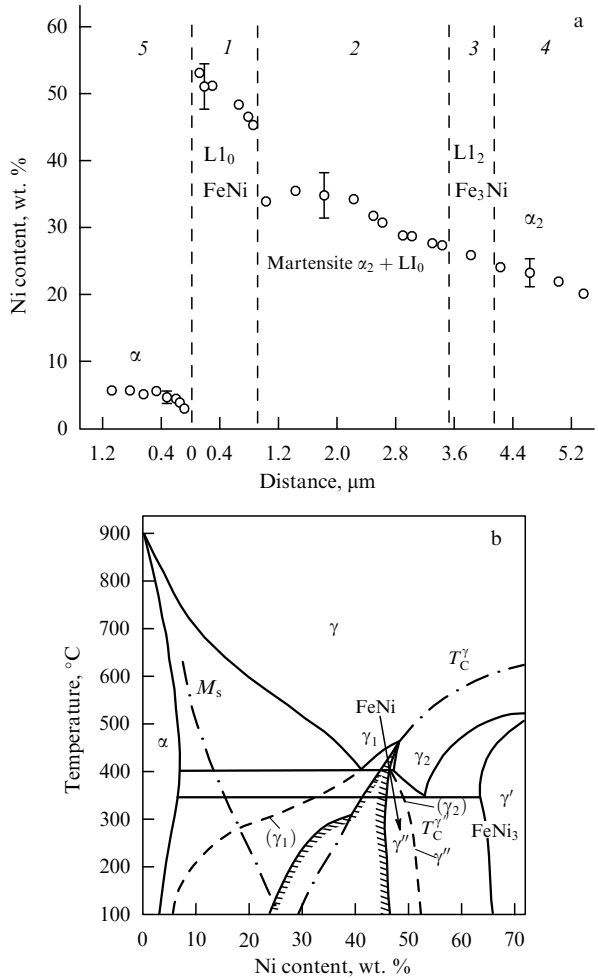

Figure 8. (a) Diagram illustrating the presence of phases discovered in a meteorite (reproduced from Ref. [28]): (*1*) ordered FeNi phase (γ'') in the region of compositions from 45.6 to 51.4 wt.% Ni; (*2*) two-phase field: ordered γ''-FeNi phase with a Ni content of 50.9 wt.% and α_2-martensite; (*3*) ordered phase with a composition close to Fe_3Ni; (*4*) α_2-martensite with the content of ~ 25 wt.% Ni; (*5*) bcc phase with 4 wt.% Ni. (b) Phase diagram (reproduced from Ref. [29]) constructed on the basis of the analysis of the structure of meteorites and an allowance for the results of thermodynamic calculations [20, 21], which take into account contributions from magnetic and chemical interactions. *M* stands for the temperature of the martensitic transformation. The dashed lines limit the miscibility gap between the paramagnetic and ferromagnetic $\gamma_1 + \gamma_2$ phases. The shaded boundaries separate the region of spinodal decomposition. The diagram reflects: (i) the monotectoid reaction $\gamma_1 \rightarrow \alpha + \gamma_2$ at a temperature of approximately 400 °C, where γ_1 is a paramagnetic austenite, α is a ferrite, and γ_2 is a ferromagnetic austenite; (ii) the eutectoid reaction $\gamma_2 \rightarrow \alpha + \gamma'$ at a temperature of approximately 345 °C, where γ' is $L1_2$-type ordered phase $FeNi_3$; (iii) the miscibility gap connected with the region of spinodal decomposition (into ferromagnetic and paramagnetic austenite) at low temperatures, and (iv) the $L1_0$-FeNi phase, which is present in the diagram as metastable.

in Ref. [29]: at low temperatures, the α phase, which contains 3.6 wt.% Ni, is in equilibrium with the $\gamma'(Ni_3Fe)$ phase, which contains 65.5 wt.% Ni. The ordered $L1_0$-γ''(FeNi) phase containing 51.5 wt.% Ni, which was revealed by the authors of study [29] in the meteorite, is present in the diagram as a metastable phase (Fig. 8b). In this case, however, the reason for the absence of magnetic influence on the structure formed in the meteorites is obscure. The authors of Ref. [29] do not explain this and again superimpose a magnetic influence on the structure formed.

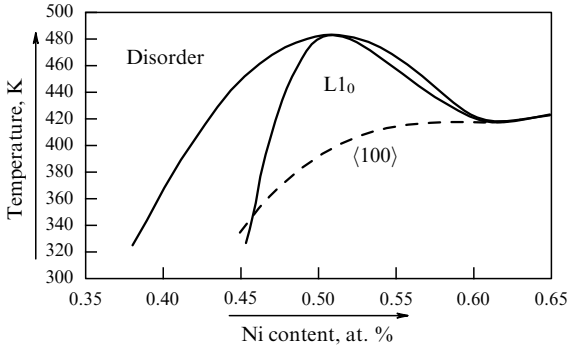

Figure 9. Fe–Ni phase diagram. (Taken from Ref. [30].)

Later on, in paper [30], a thermodynamic calculation of the Fe–Ni phase diagram was again carried out (Fig. 9). The presence of the $L1_0$-γ''(FeNi) phase is shown in the region of negative temperatures; therefore, its experimental detection was considered to be impossible. The presence of the Fe_3Ni phase again is not fitted into the calculated Fe–Ni diagram.

But there are also such calculated diagrams in which, besides the experimentally determined or tentative ordered phases $FeNi_3$-$L1_2$, Fe_3Ni-$L1_2$, and FeNi-$L1_0$, the formation of ordered Fe_2Ni and Ni_2Fe phases with a $C11_f$ superstructure proves to be possible [31].

In 2015, one more calculated diagram of phase equilibria in the Fe–Ni system was published [32]. In the last work, the formation of an $L1_0$ phase as a stable phase is stated, it being located in the region of equiatomic composition at a temperature below $\sim 230\,^{\circ}C$ (Fig. 10). The author of study [32] focuses on the representation of two different mechanisms of the disorder $\rightarrow$ ordered-$L1_0$-phase transformation. The dashed–dotted curve is the phase boundary that divides the region of the $L1_0$ phase realization into two parts, which differ in the mechanism of formation. In the high-temperature part, the ordered phase is formed via the mechanism of a first-order phase transformation that occurs via the nucleation and growth of domains of the ordered phase in the disordered matrix, whereas, at temperatures in the region lower than the dashed–dotted curve, the $L1_0$ phase is formed via a second-order mechanism, called spinodal ordering, which occurs as a result of infinitely small oscillations of atoms in the entire volume of the sample with a gradual increase in the degree of long-range order. This mechanism of ordering in the literature is called short-range ordering.

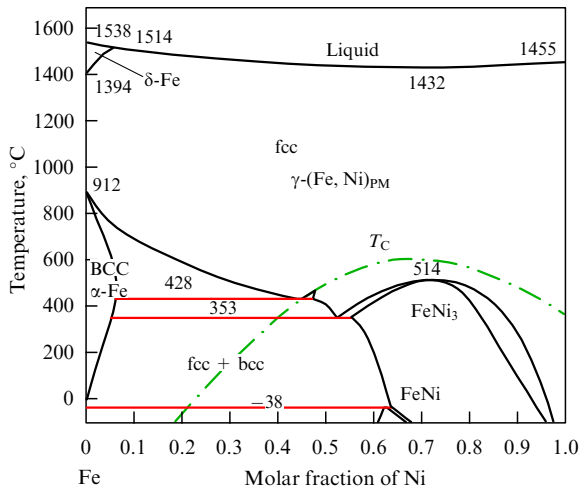

Figure 10. A1/$L1_0$ phase boundary and the position of the temperature of spinodal ordering (dashed–dotted curve). (Reported by Mohri [32].)

It should be noted, however, that the mechanism of short-range (uniformly developing in the entire volume) ordering has not been confirmed experimentally [33]. Short-range ordering features a heterogeneous character, called a microdomain ordering. Unlike atoms, even at high temperatures, are arranged predominantly in groups, forming domains with a high degree of order. The sizes of such domains decrease sharply as the temperature increases. The state of short-range order, fixed by quenching of the alloy from high temperatures, is characterized by a high level of internal elastic stresses, because of a coherent coupling of the microdomains with the matrix. This leads to a strong diffuse smearing and to a decrease in the intensity of superstructure reflections in the diffractograms. The experimental data on the formation of microdomains with a degree of order close to unity for the CuAu alloy are described in Ref. [34].

Since, thus far, the precise values of the critical temperature T_{cr} of the formation of the FeNi and Fe_3Ni phases are unknown and, moreover, the very existence of these phases is questioned, the irradiation of the alloy or its plastic deformation are frequently conducted in many studies at too low temperatures, at which the diffusion mobility of atoms is insufficient for the formation of ordered phases, or at temperatures exceeding T_{cr}, when the formation of these phases no longer occurs (see, e.g., Refs [3, 35]). Moreover, an important factor in the detection of superstructure reflections is the duration of irradiation. If the irradiation time is too short, then the ordering cannot occur. On the other hand, if the irradiation time is too prolonged, then damage to the sample can prove to be so great that the regions that were ordered can undergo disordering. The irradiation dose also influences the detection of the precipitated phase. Thus, in cases of high concentrations of nickel in the alloy, an increase in the irradiation dose first leads to a suppression of the central part of the Mössbauer spectrum, and then a paramagnetic peak appears in the spectrum [15]. These experimentally registered facts also introduce discord into the construction of the phase diagram.

If the irradiation is carried out directly in the column of an electron microscope at different temperatures, then in the state of radiation damage and poorly controlled heating temperature, significant errors can arise in the determination of critical ordering temperatures at least in the region directly subjected to irradiation. For example, an opportunity of ordering was studied [2, 4] in alloys very close to each other in composition (and also close to the composition of the alloy examined in this article): N32 and Fe–32 wt.% Ni, respectively. In spite of the fact that in both studies the alloys were prepared from high-purity components by vacuum zone melting in an argon atmosphere and the same methods of study were used, a nonconformity of the results of determining the critical ordering temperature of the discovered phase is observed: $T_{cr} = 415\,^{\circ}C$ in Ref. [2], and $T_{cr} = 270\,^{\circ}C$ in Ref. [4].

The position of T_{cr} depends on the presence of interstitial elements in the alloy. At a carbon content of 0.001%, this temperature is $T_{cr} = 470\,^{\circ}C$ [17]; at a larger carbon content (1.7%), T_{cr} can increase to $\sim 580\,^{\circ}C$.

Attention should also be drawn to the ambiguous position of the curves of the magnetic transformation (Curie temperature T_C) in the phase diagrams. In alloys with a nickel content

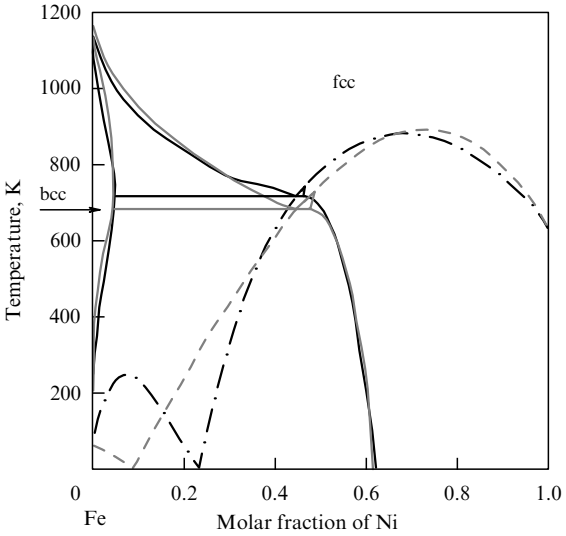

Figure 11. Magnetic phase diagram constructed taking into account the magnetic contribution to the Gibbs energy [36] in comparison with an *ab initio* calculated diagram [37]. Black curves correspond to those determined in Ref. [36]; gray lines are curves taken from the SSOL database [37]. Solid curves trace out the phase boundaries; dashed curves are lines of the magnetic transformation.

of less than 40 at.% [9, 10] (see Fig. 3), the austenite is characterized as ferromagnetic at room temperature ($T_C \approx 200\,^\circ$C); in another diagram (see Fig. 1), the curve of the Ni-content dependence of T_C is broken at a temperature above 200 °C, while in the diagrams given in Fig. 2 this curve is completely absent. In Fig. 8b, a region of the simultaneous presence (miscibility gap) of the paramagnetic and ferromagnetic phases $\gamma_1 + \gamma_2$ is shown in the region of low temperatures. In the phase diagram given in Ref. [30], which was published almost 15 years later, the miscibility gap is absent (see Fig. 9), but a curve is given of the Ni-content dependence of T_C in a wide range of compositions of Fe–Ni alloys. In Ref. [36], the curves of the magnetic transformation are compared with the position T_0 of the equilibrium boundaries of the phase fields taken from Ref. [37] (Fig. 11). At the temperature of absolute zero, the T_C curve exhibits an elbow. According to the results of calculations, the transition to the antiferromagnetic state occurs at the composition of Fe–(23–25) at.% Ni. Experimentally, the composition of the Fe–Ni alloy corresponding to the elbow has not been determined. Thus far, there have been no convincing results of the measurements of the Néel temperature T_N.

The largest discrepancy between the available experimental values of T_C in fcc alloys with the Ni content $\leqslant 30$ at.% is caused by the sharp decrease in the T_C values with a decrease in the nickel content. The reliable experimental determination of the Curie temperature for low-nickel alloys is also complicated by the development of the martensitic $\gamma \rightarrow \alpha$ transformation, which is developed at temperatures higher than room temperature. Under conditions of the two-phase state ($\gamma + \alpha$), the crystal lattice of the γ phase undergoes an elastic compression, which can affect the position of T_C and lead to the ambiguity of its values at different volume fractions of these phases.

In this article, we give experimental results from analyses of the structure of the retained austenite in the process of a slow heating of the alloy Fe–32 at.% Ni, which resides initially in the two-phase $\gamma + \alpha$ state. These experimental results, in our opinion, make it possible to give preference to the diagram constructed by Chamberod et al. [2]. Note that this diagram is not given in the reference literature.

We hope that our work will help to introduce clarity to the representation of the equilibrium phase diagram of the Fe–Ni system and in understanding the nature of Invars.

2. Material and the method of investigation

The Fe–32 at.% Ni alloy was made from high-purity components. The carbon content in it does not exceed 0.01%. After homogenization at a temperature of 1100 °C for 48 h, the alloy was sharply quenched in water. The obtained structure is characterized as roentgenographically austenitic. By electric-spark cutting, which ensures the smallest distortions of the surface layer, a sample $10 \times 10 \times 15$ mm in size was prepared. Cooling in liquid nitrogen and slow warming in air to room temperature led to the formation of an ≈ 80 % α phase of a lenticular morphology. Then, the sample placed into an evacuated ampoule was heated at a rate of 0.3 °C min^{-1} to the temperature of 400 °C, after which, together with the turned-off furnace, it was cooled to room temperature. Using electric-spark cutting, the sample was divided into two parts , and then a sample for the preparation of thin foils was cut off. The surface of the sample cut and the intermediate product for producing foils were ground using a fine-grained polishing paper.

The workpiece for the production of foils with a thickness of 0.2 mm was thinned in an electrolyte, prepared based on orthophosphoric acid with the addition of chromic anhydride and sulfuric acid, at a voltage of 25 V. The electropolishing and the electroetching of a bulky sample for studying the microstructure in a scanning electron microscope were carried out in the electrolyte, consisting of 90% glacial acetic acid and 10% perchloric acid, at a voltage of 100 V. The initial temperature of the electrolyte was 5 °C. To obtain a sharp image of the structure in the scanning electron microscope, deep etching is required, which ensures the formation of a noticeable relief on the surface of the polished section. Therefore, the time of electroetching lasted no less than 1 min. To decrease the warming-up of the sample in the zone of contact with the electrolyte, the sample was rapidly moved continuously. Immediately after electroetching, the samples were washed in an alcohol or in acetone to prevent the oxidation of the surface.

The study of the structure was carried out at the Department of Electron Microscopy of the Test Center of Nanotechnology and Advanced Materials (TC NAM) of the Institute of Metal Physics, Ural Branch of the Russian Academy of Sciences, using a JEM-200CX electron microscope at a voltage of 160 kV, and using a Quanta-200 scanning electron microscope at room temperature.

3. Results of the investigation

Figure 12a displays an SEM image of the structure obtained in the Fe–32 at.% Ni alloy after cooling in liquid nitrogen from the $\gamma + \alpha$ field. Due to a high density of defects in the crystal structure, the plates of the α phase are characterized by a high etchability and are therefore darker than the retained austenite, which makes it possible to easily distinguish martensite plates from the fragments of retained austenite. Both phases, α and γ, because of the difference in their specific volumes, undergo plastic defor-

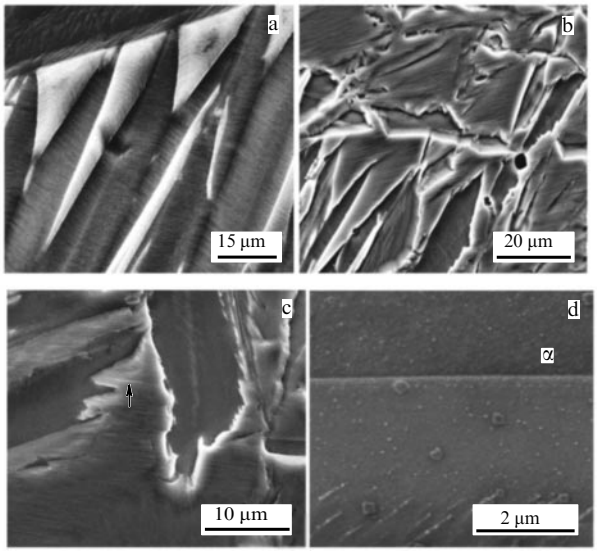

Figure 12. (a) $\alpha + \gamma$ structure of the Fe–32 at.% Ni alloy after cooling in liquid nitrogen; the γ/α phase boundaries are exceptionally flat. (b, c) The structure of the γ/α phase boundaries after slow heating to the temperature of 400 °C; the arrow indicates the trace of slip in the region of retained austenite with a high density of particles. (d) Structure of reverted austenite, which was formed in the process of a discontinuous reaction, and the γ/α phase boundary with a high density of dispersed particles.

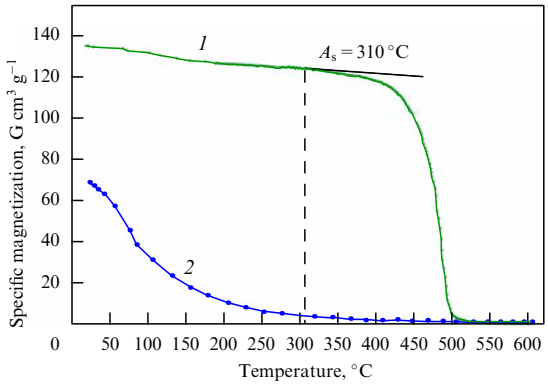

Figure 13. Change in the magnetization of the Fe–32 at.% Ni alloy in the process of slow heating at a rate of 0.3 °C min^{-1} to the temperature of 600 °C. The rate of cooling to room temperature is 4 °C min^{-1}. The temperature of the onset of the $\alpha \rightarrow \gamma$ transformation is 310 °C.

mation in the course of the $\gamma \rightarrow \alpha$ transformation. Owing to the relief on the etched surface of the polished section, the traces of deformation on the surfaces of both the α-phase plates and the fragments of retained γ-austenite are distinctly revealed. The absence of traces of deformation on the surfaces of some plates indicates only that these plates were unfavorably oriented with respect to the direction of the electron beam. A small inclination of the polished section makes visible traces of deformation in these plates as well. Structures of the alloy in the $\gamma + \alpha$ state were investigated in detail in Refs [38, 39].

The primary attention in the context of this work should be focused on the structure of the γ/α phase boundaries: they are exceptionally flat, without kinks or steps (Fig. 12a).

In Fig. 12b, c, an image is given of the structure of a sample that underwent slow heating at a rate of 0.3 °C min^{-1} to the temperature of 400 °C. The phase boundaries substantially changed their configuration; they became crystallographically uneven, with numerous kinks and protrusions. The observed change in the structure of the alloy indicates the development of an $\alpha \rightarrow \gamma$ transformation by means of the migration of the boundaries of retained austenite to the side of the α phase. In Fig. 13, a change is shown in the magnetization of the same sample in the process of heating at the same rate. The deviation of the magnetization curve from a linear behavior begins at a temperature of 310 °C. This temperature should be considered as the temperature A_s of the start of the reverse transformation. The smooth decrease in magnetization in the process of heating to 400 °C — in the lower part of the temperature interval of the reverse $\alpha \rightarrow \gamma$ transformation — confirms the diffusion mechanism of the structure formation in the reverted austenite.

An analogous phenomenon was registered in paper [40] with the aid of an interference microscope (Fig. 14a), and by the metallography technique in paper [41] (Fig. 14b). The plates of martensite after heating to a temperature of 400 °C are fringed with a narrow layer of reverted austenite. A

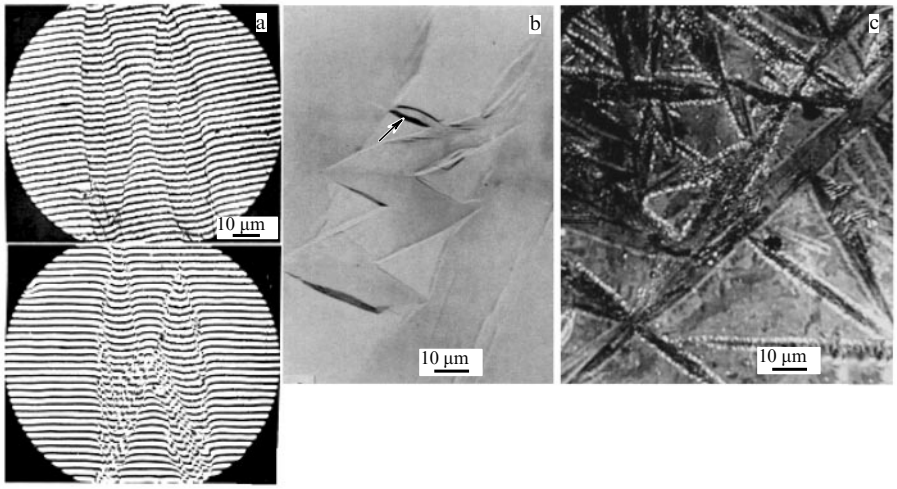

Figure 14. Diffusion-assisted development of the $\alpha \rightarrow \gamma$ transformation by means of the migration of the γ/α phase boundary revealed: (a) using an interference microscope [40]; (b) from the formation of a relief around interphase boundaries [41], and (c) based on the development of discontinuous decomposition with the precipitation of the Ni_3Ti phase in the Fe–NiTi alloy [42, 43].

similar phenomenon was discovered in our earlier work devoted to a study of the initial stage of the reverse $\alpha \rightarrow \gamma$ transformation in the metastable Fe–Ni–Ti alloys [42, 43]. This stage is easily revealed even in an optical study of the structure, since it is accompanied by the decomposition of the austenite with the precipitation of an η-phase Ni_3Ti (Fig. 14c), which unambiguously confirms the diffusion-controlled mechanism of the $\alpha \rightarrow \gamma$ transformation at its initial stage.

The formation of a relief on the preliminarily polished and etched section surface around the plates of martensite (Fig. 14b) reflects the reality of a change in the volume of the region that underwent the $\alpha \rightarrow \gamma$ transformation and is not the sign of an exceptionally shearwise process.

In the retained austenite, fine particles densely located on the slip traces (indicated by arrows in Fig. 12c) are visible. In Fig. 12d, an image of a region near the boundary between retained austenite and martensite is given at a large magnification. Particles of a new phase are distinctly visible, which unambiguously indicates that the decomposition of austenite into two phases has occurred. The large particles have a square faceting. The cubic shape of the particles testifies to the isomorphism of the particles and the matrix, and to a small difference in the lattice parameters. It is important to note that the slip traces do not reach the interface between the γ and α phases. A region free of slip traces can be seen, with chaotically located large particles of the new phase. In the upper part of Fig. 12d, the boundary between austenite and martensite (darker region) is seen. Particles of the precipitated phase can also be seen in the martensite. The migration of the interphase boundary caused by the development of the $\alpha \rightarrow \gamma$ transformation leads to collisions between these particles and their coalescence at the migrating boundaries. Because of the low surface energy of particles, the migrating boundary proves to be able to become detached from them and to move further into the depth of the martensite plate. In this case, the reverted austenite remains behind the front of migration, as do large particles of the precipitated phase, which were formed in the process of slow heating from the temperature of the origin of the reverse $\alpha \rightarrow \gamma$ transformation under the action of the discontinuous (diffusion) mechanism.

It is well known that discontinuous reactions lead to the formation of phases close to equilibrium, with the indispensable participation of recrystallization of the matrix and its orientation corresponding to the orientation of the grain, whose boundary migrates. As can be seen from the phase diagram presented in Fig. 2b, the equilibrium γ phase at a temperature of 400 °C must contain $\sim$ 35% Ni or, according to the diagram given in Fig. 8b, 40%, whereas, according to the diagram shown in Fig. 11, it can contain up to $\sim$ 50% Ni. Thus, according to any of the earlier known phase diagrams, the γ-matrix must contain a larger amount of nickel than there is in the composition of the alloy investigated. Therefore, the very fact of detecting the discontinuous reaction makes it possible to assert that the precipitated phase is Fe_3Ni. Only the precipitation of this phase with an enhanced content of iron in comparison with that in the matrix makes possible the fluctuational nucleation of the equilibrium γ phase, enriched in nickel near the γ/α interface, necessary for the formation of a nucleus of a discontinuous reaction.

Thus, the equilibrium state of the Fe–32 at.% Ni alloy realized via a diffusion process at a temperature of 400 °C corresponds to an $Fe_3Ni + \gamma$ phase composition. This experimental result gives grounds to assume that the most reliable phase diagram is that presented in Fig. 2b.

An attempt to carry out a quantitative analysis of the contents of nickel and iron in the precipitated phase using a Quanta-200 scanning electron microscope proved to be unsuccessful, since the electron probe, whose diameter was an order of magnitude larger than the average size of precipitates, affected not only the particle, but also the surrounding matrix. Moreover, a quantitative analysis of the composition of dispersed precipitates with a size less than 1 μm in bulk samples can be carried out only in the case of the absence of the elements to be analyzed in the matrix [44].

It is should be admitted that in our case it is impossible to completely realize an equilibrium two-phase state at a temperature of 400 °C in the entire volume of the alloy. The reason is the following. The discontinuous reaction, which leads to the equilibrium state, is initiated by the driving force of the reverse $\alpha \rightarrow \gamma$ transformation. The establishment of the necessary ratio between the numbers of Fe and Ni atoms in the γ and α phases requires a redistribution of the atoms between these phases according to any published phase diagram. The mobility of the γ/α phase boundaries originally free of Fe_3Ni-phase particles subsequently proves to be suppressed because of the accumulation of particles on the boundaries. This fact is well illustrated by Fig. 12d: the density of the location of particles at the phase boundaries is great. With an increase in the degree of migration of the γ/α phase boundaries, the near-boundary region of martensite plates is depleted of nickel; correspondingly, the length of the diffusion paths of nickel atoms to the migrating boundaries from the bulk of martensite plates increases. This process occurs via the bulk diffusion of nickel, whose rate is several orders of magnitude less than the diffusion rate over grain boundaries [45–49]. Therefore, because of a decrease in the mobility of the γ/α phase boundaries and the deficiency in nickel atoms supplied via bulk diffusion to the migrating boundary, the equilibrium phase Fe–40 at.% Ni no longer can be formed, and the development of the discontinuous reaction of the $\alpha \rightarrow \gamma$ transformation ceases.

When studying the structure of similar regions with the aid of a transmission electron microscope, additional nuances of the development of phase transformations in austenite have been discovered. The analysis of the structure of austenite in a thin foil (Figs 15a–f) is complicated by the presence of laths of surface martensite, which are visible as unidirectional dark bands on the bright-field image of the structure (Fig. 15a).

The corresponding electron diffraction patterns are complicated (Fig. 15b). Their detailed interpretation, which includes the analysis of the structure of surface martensite, is the subject of future studies. Now, we note only that the orientation of the martensite laths corresponds to the $[111]\alpha$ zone axis marked by dashed lines in Fig. 15b.

Let us perform a detailed analysis of the structure of the γ phase. In the electron diffraction pattern, the $[12\bar{5}]$ zone axis is designated. In Figs 15c–g, dark-field images are shown of the structure taken in the reflection 311 of the γ phase under various small changes in the inclination of the foil. The 311 reflection is double. The splitting of the reflection into two closely spaced reflections can be clearly seen in the case of the reflection $\bar{1}31$, which belongs only to the $[12\bar{5}]$ zone axis. This gives the opportunity to obtain different dark-field images of the structure caused predominantly by one of these reflections. The image in Fig. 15c corresponds to the precipitated phase Fe_3Ni, which follows from the presence of

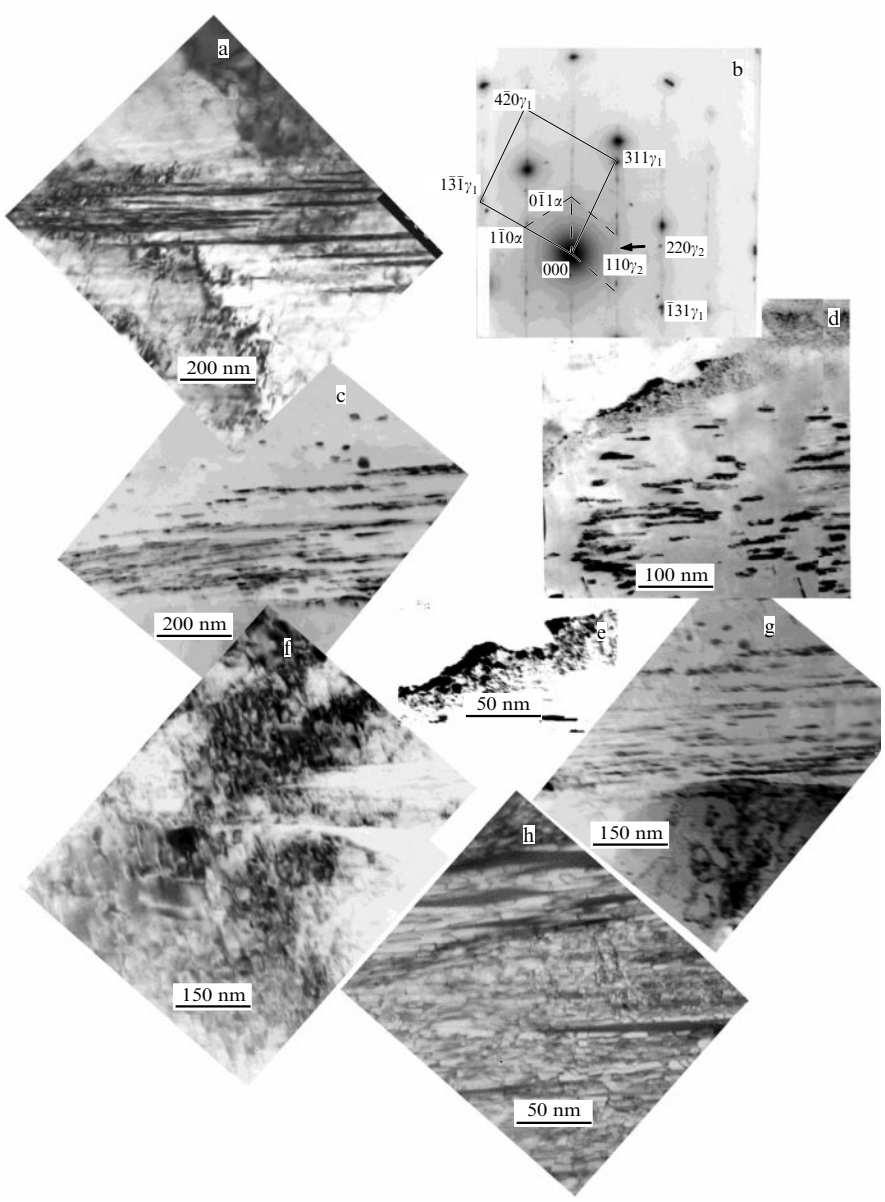

Figure 15. Images of the structure of retained austenite after heating at a rate of 0.3 °C min^{-1} to a temperature of 400 °C and cooling down to room temperature in a turned-off furnace. (a) Bright-field image. (b) Corresponding electron diffraction pattern: in the center, reflection 311 consisting of two closely spaced reflections, which can be seen distinctly in the case of reflection $\bar{1}31$; for which two zone axes are indicated: $[12\bar{5}]\gamma_1$ and $[111]\alpha$ of the lath surface martensite. (c–e) Dark-field images of the structure in one of the 311 reflections located farther from the zero spot: (c) the central part of the fragment which contains predominantly the structure of surface martensite; (d) the near-boundary region with an α plate; and (e) the same, at a greater magnification. (f, g) Dark-field images of the structure after inclination of the foil by $\sim 1°$ in the reflection 311 located (f) nearer to the zero spot and (g) farther from the zero spot. (h) Dark-field image of the structure in the $110\gamma_2$ reflection (indicated by an arrow), which lies in the same systematic row as the reflection $220\gamma_2$.

particles near the martensite laths. At sites of the intersection by shear planes, the particles are 'spread' along these planes; as a result, the reflection acquires a noticeable azimuthal smearing. The increased angular arrangement of the azimuthally smeared reflection indicates that the lattice parameter of the Fe_3Ni phase is less than the lattice parameter of the surrounding fcc matrix.

Figure 15d displays a dark-field image of the structure of the region that directly adjoins the γ/α interphase boundary. This region was formed at the final stage of the discontinuous formation reaction of the two-phase $Fe_3Ni + \gamma$ region, which is a reaction of discontinuous decomposition, rather than discontinuous coagulation. Its growth is ensured exclusively due to the supply of nickel atoms from the bulk of the α-phase plates. The structure of this region at a larger magnification is shown in Fig. 15e. Morphologically, such a picture of discontinuous decomposition is analogous to the precipitation of the coherent Ni_3Ti-γ' phase in Fe–Ni–Ti alloys [42, 43]: the Fe_3Ni phase has the shape of rods, which are branched in the course of growing a colony for the retention of a constant interlamellar distance. Such a morphological picture of the colony of discontinuous decomposition is only possible upon precipitation of an isomorphous phase coherently connected with the matrix of particles. Based on this analogy, we conclude that, by means of the discontinuous mechanism, a coherent fcc phase ordered according to the $L1_2$ type precipitates in the fcc matrix with an only slightly different lattice parameter. In the case of the precipitation of

a phase ordered according to the $L1_0$ type, such a structure of discontinuous precipitation could not be formed, since the branching of the phase is only possible for an isomorphous structure of the phases in the colonies of discontinuous decomposition.

Thus, the development of the reverse $\alpha \rightarrow \gamma$ transformation in the course of slow heating occurs via a mechanism of the discontinuous reaction, the rate of which decreases with an increase in the degree of its development. At the beginning of the development, the reaction rate is controlled by the processes developing at the interfaces between the γ and α phases and occurs via the joint motion of the interphase boundaries together with the particles; and at the final stage, it is controlled by the rate of the supply of nickel atoms from the bulk of the α phase to the migrating boundary. The obtained experimental results completely agree with the experimental data and theoretical predictions presented in Refs [48, 49].

The inclination of the foil in the electron microscope revealed additional evidence of presenting the mechanism of the development of phase transformations in fragments of the retained austenite. Figure 15f displays the same region of the foil. The acting reflection proved to be the 311 reflection having an equiaxed shape, which is located nearer to the 000 reflection, i.e., corresponding to a phase with a larger parameter of the crystal lattice located around the martensite laths. This phase has a sufficiently clearly pronounced cellular internal structure with a high level of elastic distortions. This follows from the presence of a noticeable relief and disclination-induced turns, which lead to diffraction effects with a nonuniform intensity. In the lower left-hand corner of Fig. 15f there is a partial disclination with a practically complete absence of structure. An additional insignificant inclination of the foil led to the image of the structure presented in Fig. 15g. In the reflecting position, there again proved to be Fe_3Ni particles, just as in Fig. 15c, and, furthermore, the region of the partial disclination (in the right-hand part of the figure) proved to be in the reflecting position. Dispersed particles of the Fe_3Ni phase are distinctly visible at the boundaries of the cells.

The image displayed in Fig. 15g suggests that the structure comprises an ordered $L1_0$ matrix of composition FeNi, and that dispersed particles of Fe_3Ni are located at the boundaries of its domains. In the growth process of the domains of the matrix, which is ordered according to the $L1_0$ type, a rejection of the excess element — iron — into the domain boundaries occurs. After reaching the necessary chemical composition in the interlayers of the disordered matrix, particles of the Fe_3Ni phase are formed between the domains. An analogous situation was observed in our studies [50, 51] upon the investigation of ordering in the Cu–Au–Ag and Cu–Au–Pt alloys. The largest local deformation of the aged and ordered alloy is concentrated at the domain boundaries; it is precisely for this reason that they are visible in the structural reflections of the matrix (Fig. 15g). The existence of a local deformation of the crystal lattice at the thermal antiphase boundaries (APBs) in ordered alloys, caused by the presence of an enhanced concentration of one of the components of the alloy, has been experimentally shown in Ref. [52].

Since the $[12\bar{5}]$ zone axis does not contain superstructure reflections, an attempt was made to obtain a dark-field image of the structure in the 110 reflection (indicated by an arrow in Fig. 15b), located in the same systematic row as the $220\gamma_2$ reflection. Figure 15h represents the dark-field image of the structure located between the martensite laths. In the lower part of Fig. 15h, some boundaries have a significant thickness. This means that the domains are separated from each other by interlayers of the disordered matrix, rather than by APBs. In the upper part of Fig. 15h, the APBs have a glomerular morphology and do not contain particles of the precipitated phase. The disappearance of the interlayers of the disordered matrix occurs in the process of the coagulation of $L1_0$-FeNi domains. The APBs pass over the particles of the precipitated phase, which turn out to be located in the bulk of growing domains. This reaction occurred in the thinnest part of the foil, where, owing to a significant gradient of elastic stresses, the migration of APBs, apparently, occurred in the process of preparation of the foil or its storing at room temperature. The size of antiphase domains is by an order of magnitude greater than the size of domains in the thick parts of the foil. A similar behavior was observed in the experimental study of the structure in Cu–Au–Pt alloys [52]. The presence of domain boundaries of the glomerular morphology in the upper part of Fig. 15h removes all doubt relative to the ordered state of the matrix. The equilibrium state of Fe–32 at.% Ni at room temperature—FeNi-$L1_0$ and Fe_3Ni-$L1_2$—completely corresponds to the phase diagram shown in Fig. 2b [2] constructed (based on the experimental study of alloys prepared by zone melting with the content of nickel from 27 to 50 wt.%) with the use of different methods of study. This diagram is in agreement with the results of the present investigation and seems to be the most reliable.

4. Discussion of results

The experimental results presented in this review were obtained based on the study of the initially two-phase $\alpha + \gamma$ structure. The results are mainly related to the analysis of the structure of retained austenite, which underwent slow heating to the temperature of 400 °C and cooling, together with the turned-off furnace, to room temperature. In the literature, no such studies are available. An important difference from all previous studies is the fact that under the conditions of a two-phase state an additional driving force appears, which stimulates the formation of reverted austenite and determines the concrete vector of its formation, which substantially facilitates the search for the fragments of the structure that correspond to the equilibrium phase state and makes it possible to sufficiently reliably establish its phase composition. The registering of the complex discontinuous reaction of the $\alpha \rightarrow \gamma$ transformation, which is developed under the action of the diffusion mechanism, made it possible to establish and to reliably define the equilibrium phases that are formed in the zone of the development of this reaction: reverted γ austenite + $L1_2$-Fe_3Ni. According to all existing Fe–Ni phase diagrams, the content of nickel in the arising reverted austenite must exceed its average content in the alloy; therefore, the γ phase is ferromagnetic and its Curie temperature is higher than that of the uniform initial austenite of the Fe–32 at.% Ni alloy investigated. The cooling of the alloy to room temperature leads to the development of an ordering of the matrix according to the $L1_0$ type. Thus, the reverted austenite of the Invar alloy Fe–32 at.% Ni has the equilibrium phase composition: $L1_0$-FeNi and $L1_2$-Fe_3Ni at room temperature, since its formation occurred exceptionally via diffusion processes.

This conclusion is confirmed by the Mössbauer spectra (see Fig. 5) published in Refs [2, 15]. They show the presence of two different structures in the samples after their irradiation at room temperature. In the Fe–30 at.% Ni alloy, a paramagnetic peak exists immediately after quenching. With an increase in irradiation dose, this peak becomes sharper and resides in the matrix, together with the sufficiently distinct six peaks of the ferromagnetic matrix, which indicates the development of the decomposition of the ferromagnetic austenite with the precipitation of the paramagnetic Fe_3Ni phase. With an increase in the irradiation dose of the Fe–35 at.% Ni alloy, the Mössbauer spectrum of the ferromagnetic component is characterized, apart from a strengthening of the intensity of the paramagnetic peak, by the values of the internal field and quadrupole splitting that correspond to the $L1_0$ superstructure, which testifies to the development of the tandem of Fe_3Ni + FeNi ($L1_2 + L1_0$) phases.

The Mössbauer spectra of the Fe–30 % Ni alloy [2] obtained at room temperature after irradiation are not changed with the use of a preliminary cooling of the sample to the temperature of 4 K. Moreover, the spectrum recorded at a temperature of 4 K contains a central peak, in addition to the six spectral lines. These results mean that the regions rich in iron are paramagnetic at temperatures up to 4 K and do not undergo martensitic transformation. Consequently, the structure of these regions is energetically more stable than the martensitic phase and can correspond only to an ordered structure.

It is well known that the martensite being formed upon cooling binary Fe–Ni alloys with a nickel content of less than 32 at.% to the temperature of liquid nitrogen is characterized by a crystal lattice with a tetragonal distortion [53]. It is obvious that the tetragonal distortions are caused precisely by the presence of $L1_2$ particles of Fe_3Ni coherently coupled with the martensite lattice. There is every reason to consider that the mechanism of creating the tetragonality of the martensite crystal lattice in Fe–(32–30) at.% Ni alloys is the same as in Fe–Ni–Ti alloys, in which the martensite contains coherently coupled with its matrix particles of the intermetallic compound Ni_3Ti [54– 56].

To confirm the conclusion drawn about the realization of an equilibrium phase state at room temperature in alloys of the Invar composition — $L1_0$-FeNi and $L1_2$-Fe_3Ni — let us analyze the experimental results published in Ref. [57]. The use of severe plastic deformation of the alloy Fe–36 at.% Ni (to $\varepsilon = \ln(l/l_0) \sim 7$) and subsequent annealing at temperatures of 260–480 °C led to a change in the structure of the boundaries of the fragments produced by the deformation: they became thinner and clearer, with their misorientation increasing. The authors of Ref. [57] also registered the precipitation of an ordered phase near and at the boundaries of the fine-grained structure and a simultaneous increase in the saturation magnetization of the sample. Consequently, the precipitation of this phase is stimulated by the conversion of nonequilibrium boundaries into equilibrium ones as a result of the migration of boundaries and the development of a discontinuous reaction. Referring to the diagram presented in Fig. 3a, the authors of Ref. [57] connect their results with the precipitation of an $L1_2$ ordered ferromagnetic phase Ni_3Fe with $T_C = 610$ °C and assume that an increase in the magnetization is precisely due to the precipitation of this phase (Figs 16a, b). However, as can be seen from Fig. 16c, the restoration of the level of magnetization that corresponds to the initial single-phase alloy Fe–36 at.% Ni occurs after

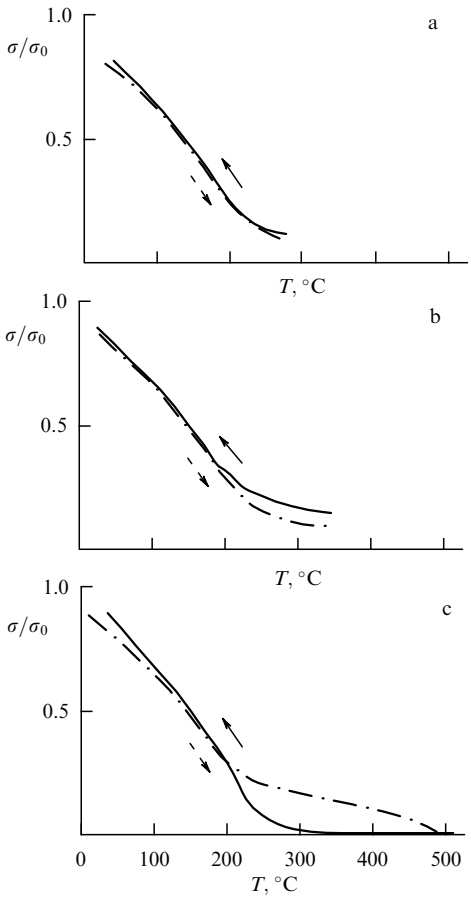

Figure 16. Curves of the change in the saturation magnetization of a sample of the Fe–36 at.% Ni alloy subjected to severe plastic deformation, obtained upon a sequential increase in the temperature of measurements to (a) 280 °C, (b) 350 °C, and (c) 500 °; σ_0 is the saturation magnetization of the alloy in a coarse-grained state at room temperature obtained after annealing at a temperature of 500 °C. (Taken from Ref. [53].)

heating to the temperature of 500 °C, i.e., lower than the T_C of the Ni_3Fe composition. The critical ordering temperature of the Fe_3Ni phase with an admixture of carbon is, according to the data from Ref. [17], 470 °C. (In Ref. [57], neither the precise chemical composition of the alloy investigated nor the heating rate in the magnetometric study is indicated.) Therefore, there is every reason to assume that, upon heating to the temperature of 500 °C, a disordering of the precipitated Fe_3Ni phase occurs, the state of the uniform solid solution is restored, and the chemical composition of the alloy returns to the initial state with the Curie temperature of 260 °C. The increase in T_C after annealing at 260–350 °C (Figs 16a, b) is due to the precipitation of the paramagnetic Fe_3Ni phase, by an increase in the magnetization of the γ phase enriched in nickel, and by its possible ordering according to the $L1_0$ type in the regions of discontinuous decomposition.

Thus, the results of the application of two methods of study in Ref. [57] for the recognition of the interconnected processes of the precipitation of the ordered phase and change in the magnetization of the sample confirm the validity of the phase diagram presented in Fig. 2b.

5. Nature of the Invar effect

A clear understanding of the nature of the Invar effect remains absent to date [58–66]. In many studies, which are

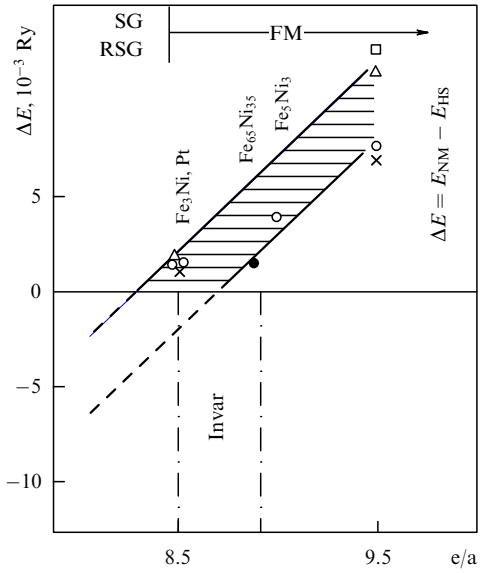

Figure 17. Difference between energies of the nonmagnetic (NM) and high-spin (HS) states, $\Delta E = E_{NM} - E_{HS}$, for the case of a ferromagnetic (FM) order [59]. SG (spin glass) is the region of ideal spin glass; RSG (reentrant spin glass) is the region of the so-called reentrant spin glass (spin glass with an antiferromagnetic interaction).

distinguished by theoretical approaches and assumptions, at present a model is being developed of a magnetically inhomogeneous ferromagnetic material with numerous fine magnetic configurations, which energetically are very close to each other. Analyzing the parameters of the pairwise exchange interaction, the authors of Refs [59–66] come to the conclusion that the origin of magnetic dispersion can be caused by the extreme sensitivity of the exchange interaction of an atom with the surrounding atoms. The greatest correspondence of the theoretical representation of the structure of a ferromagnet with the experimental results is observed when the model is based on the assumption of the presence of a short-range order in the structure of the alloy, which is manifested already in the first two coordination spheres.

Wassermann [59] carried out a theoretical generalization of experimental results obtained for different Invar alloys. We dwell only on those results that concern the Invar alloys of the Fe–Ni system. Figure 17 presents the results of a theoretical calculation of an energy difference between the nonmagnetic (NM) and high-spin (HS) states, $\Delta E = E_{NM} - E_{HS}$, for the case of a ferromagnetic (FM) order. Figure 18 shows the change in the physical properties depending on the number of electrons per atom of the alloy, e/a. This number is proportional to the change in the chemical composition of the alloy and to its lattice parameter. Therefore, a change in the chemical composition of the alloy is given on the abscissa axis, in addition to a change in e/a.

All the alloys and compounds with the e/a values within the borders of the shaded region (see Figs 17 and 18a) are stable fcc ferromagnets. For example, at e/a ~ 9, the difference ΔE between the energies of the FM (or HS) and NM states is large and positive. The critical pressure p_c necessary for the transformation of an FM state into the NM state ($p_c = -2\Delta E/\Delta V$ [61]) is also large. These systems do not manifest magnetovolume effects caused by the

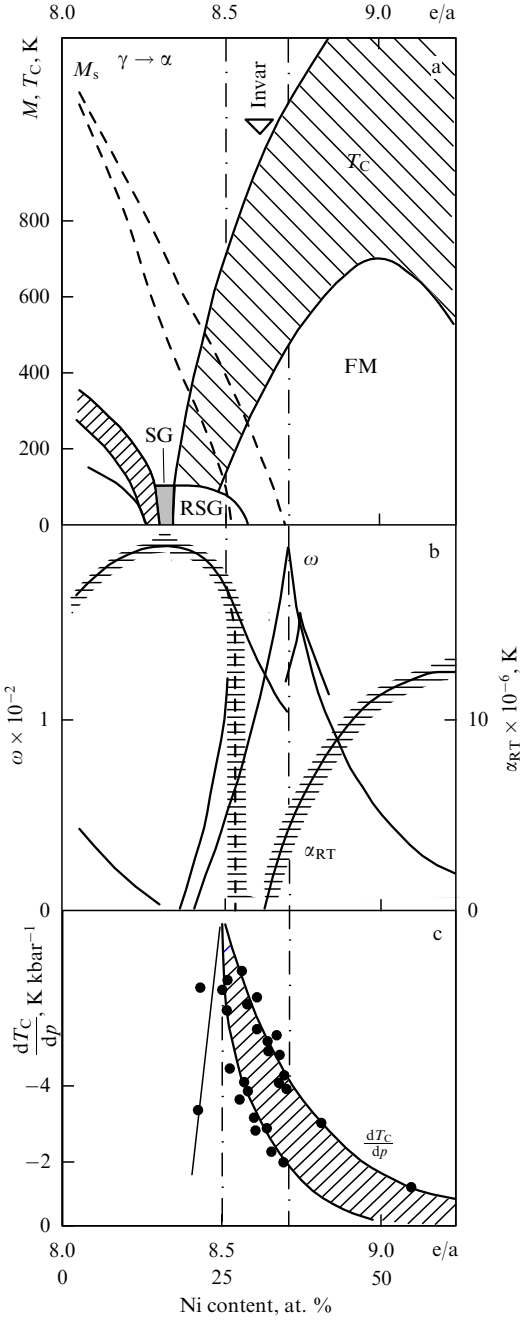

Figure 18. Different experimentally determined physical quantities depending on the electron concentration per atom, e/a, for fcc alloys of 3d metals [59]. M_s is the temperature of the onset of the martensitic transformation; ω is the magnetostriction; α_{RT} is the thermal expansion coefficient, and p is pressure.

influence of magnetostriction ω(e/a), or manifest them very weakly (Fig. 18b). In the range of $8.5 <$ e/a < 8.7, the energy difference ΔE remains positive; consequently, the systems are ferromagnetic, but the absolute values of ΔE and p_c are small. Therefore, the systems in this region of Fe and Ni concentrations reveal a large magnetic moment–volume instability. Experimentally, this is manifested in a large volume of spontaneous magnetostriction ω(e/a) (Fig. 18b). In this case, as shown in Fig. 18c, the maxima of ω (minima of the thermal expansion coefficient α_{RT}) are accompanied by maxima in the dependence of the derivative of the Curie temperature on pressure, dT_C/dp.

Under normal conditions, the magnetic moment of atoms in ferromagnetic materials decreases with decreasing volume. The Curie temperature T_C decreases with a decrease in the lattice parameter. However, the magnetostriction is large in the Invar region (Fig. 18b); therefore, in spite of an increase in the volume, the average value of T_C decreases (Fig. 18a) — this is the essence of the anomalous behavior of Invars. An increase in the volume is accompanied by a decrease in the magnetization or by a decrease in the magnetic moment of atom, which is the same thing. The almost quantitative agreement between the results of experiment (see Fig. 18) and theory (see Fig. 17) allowed the author of Ref. [59] to draw a conclusion that it is the magnetovolume changes occurring in the range of Fe–Ni Invars that are responsible for the anomalous behavior of many important physical and structural properties, as well as for the emergence of an Invar effect.

For an explanation, the author of Ref. [59] invokes the examination of the Fe_3Ni composition, which does not lie in the range of Invar alloys.

The calculation of the energy of the FM $\rightarrow$ NM transformation for this composition showed that the magnetic moment of atoms and their volume change in parallel, nonanomalously: the volume of an atom decreases with a decrease in the magnetic moment. It is sufficient to apply a small pressure for the Fe_3Ni phase to become nonmagnetic. The magnetic moments of atoms in FeNi and in pure Ni are stable. The NM state can be achieved in experiments only at technically unreal high pressures. This different response to the external pressure of the Fe_3Ni composition and of alloys with a near-boundary but higher content of nickel is the key to understanding the nature of Invars [59]. No direct experimental proof of the fact that a phase of Fe_3Ni composition is resided in the range of Invars has been given up to now, however.

If, based on the experimental results of this work, we assume that the most correct phase diagram is that presented in Fig. 2b and take into account the opportunity to develop phase transformations according to the spinodal mechanism (see Figs 1, 8b, 10), then we can make an assumption about the structure of the alloys with an Invar composition that is formed in the process of quenching from high temperatures to room temperature.

Let us examine the influence of the thermodynamic driving force determined by the values of critical temperatures T_C and T_{cr} on the phase composition of the alloy that is formed in the process of quenching. The energy of the exchange magnetic interaction between the atoms and the energy of ordering of atoms are proportional to appropriate critical temperatures. Since the T_C of the iron–nickel alloy of the equiatomic composition ($T_C = 612\,^\circ$C) is higher than the temperature of the formation of the ordered FeNi-$L1_0$ phase ($T_{cr} = 320\,^\circ$C [2] or $210\,^\circ$C [32]), the size of the critical nucleus of a ferromagnetically ordered FeNi cluster is less than that of the critical nucleus of $L1_0$ ordering. Therefore, the formation of the ferromagnetically ordered FeNi clusters with an fcc lattice and a composition close to equiatomic seems to be preferable.

The critical temperature of the formation of the nuclei of the ordered Fe_3Ni-$L1_2$ phase is less — 412–470 °C (according to data from various authors) — but is substantially higher than T_{cr} of the FeNi-$L1_0$ phase. Taking into account these data and the results of Mössbauer experiments (see Fig. 5), it can be concluded that the structure formed as a result of quenching should be characterized by the presence of dispersed ferromagnetically ordered FeNi domains, T_C of which is close to 612 °C, and of Fe_3Ni microdomains with a high degree of ordering, located in the disordered ferromagnetic matrix. This follows from the noticeable width and asymmetry of the peaks of the ferromagnetic phase and the presence of a peak of a paramagnetic phase in the Mössbauer spectra [15, 67]. It is precisely the microdomains of these structural components that are local magnetic configurations, some of which are paramagnetic and others ferromagnetic.

The estimation of the size of ferromagnetically ordered clusters that are formed in steels of grades 40Kh2N20 and 50Kh2N22 in the process of quenching, which was determined based on the magnetic moment under the assumption of their spherical shape, gave a value $d_{av} = 0.1$ nm [68]. The clusters are coherently coupled with the lattice of the matrix. The region of the elastic joining of the clusters and the matrix, which is under the conditions of a gradient compression, is characterized by a curvature of the lattice [69], in which the lattice parameter of the cluster changes gradually into the lattice parameter of the matrix. In this zone, the forces of the exchange magnetic interaction between the atoms differ from those in the matrix and in the clusters; therefore, the transition to the paramagnetic state upon heating does not occur abruptly at some specific temperature but is smeared over a temperature range. The fact of smearing of the Curie temperature was registered in Ref. [70]. In Refs [70, 71], it was shown for the example of Kh12N30 and Kh12N40 alloys that ferromagnetically ordered (superparamagnetic) clusters upon heating to the temperature of $\sim 200\,^\circ$C become paramagnetic, but during the subsequent cooling to 20 °C restore their magnetic properties. This effect is qualitatively similar to the shape-memory effect in the $\gamma \rightarrow \alpha \rightarrow \gamma$ transformation, when the elastic coherent stresses, which appear at the phase boundary between the austenite and the deformation-induced martensite, relax upon heating of the alloy, returning the initial shape to the material.

An increase in the annealing temperature leads to a progressive irreversible elimination of 'ferromagnetization' — to the disappearance of Invar properties. It is important that the complete restoration of magnetic properties, which is observed after annealing at a temperature of 600 °C [70], i.e., very close to T_C of the equiatomic FeNi alloy, testifies in favor of the assumption about the formation of ferromagnetically ordered clusters with the equiatomic composition in the process of quenching from high temperatures.

In our opinion, the alloy retains its Invar properties until the fcc crystal lattice of the ferromagnetically ordered clusters and their coherent coupling with the matrix is retained, which causes the presence of a gradient of directional elastic distortions of the crystal lattice from the fcc clusters to the fcc matrix. An increase in the size of a cluster with an increase in the temperature is accompanied by the rejection of an excess number of iron atoms (for retaining the composition of clusters that corresponds to the equiatomic one) into the surrounding elastically stressed matrix. This creates favorable conditions for the nucleation of the Fe_3Ni phase owing not only to an increase in the content of iron, but also to the compression of the crystal lattice of the matrix around the FeNi cluster, which appears as a result of specific volume differences between the matrix and the arising clusters. In this case, the Fe_3Ni phase reliably becomes paramagnetic, since the conditions for its formation are equivalent to the

conditions that appear upon application of pressure [59] (Fig. 18c). A tandem of two structural components appears: upon repeated heating or upon increasing the temperature, a growth of one nucleus will favor the growth of the other.

So, the enrichment of the matrix, which is adjacent to the Fe_3Ni particle, in nickel atoms favors the formation in it of FeNi clusters, as on a substrate. The growth of FeNi clusters, which is accompanied by the rejection of the excess iron atoms to the domain boundary, creates conditions for the nucleation of new Fe_3Ni particles on its boundary. A small increase in temperature will lead to an increase in the volume fraction of both structural components. An autocatalytic reaction will begin to develop: an FeNi domain will be nucleated and grow at the boundary of the Fe_3Ni domain. An increase in the volume fraction of the ferromagnetic FeNi clusters, which are characterized by a larger lattice parameter than that of the initial Fe–Ni composition, will lead to a growth of magnetostriction, but the accompanying process of the nucleation and growth of the paramagnetic Fe_3Ni-$L1_2$ particles, which are characterized by a smaller lattice parameter, will level off the increasing magnetostriction.

Upon cooling of the alloy to room temperature, the clusters can be returned to the ferromagnetic state with the initial magnetization, whereas the particles of Fe_3Ni, which is a stable phase, will not experience any changes. This will lead to a change in the initial structural state of the matrix: an increase in the content of nickel. Upon repeated realization of the same scheme of heating of the alloy, the ferromagnetically ordered clusters will reach larger sizes, since the difference in the lattice parameters of the matrix and cluster will be less and, therefore, the level of the directional elastic stresses will be less as well. Those clusters which will reach the critical size of the nucleus of the ordered FeNi-$L1_0$ phase will retain their structure upon subsequent cooling. Even under conditions of retaining the coherent coupling of the fct particles of FeNi-$L1_0$ with the surrounding fcc matrix, the curvature of the crystal lattice in the zone of elastic joining will change, which will lead to a change in the picture of the distribution of the directional elastic stresses. Upon cooling of the alloy to room temperature, no restoration of magnetic characteristics will occur. The anomalous Invar characteristics of the alloy will disappear.

Since the diffusion mobility of the iron and nickel atoms at temperatures lower than 250 °C is small, the alloys can work as Invars — to preserve a constant thermal expansion coefficient — for a sufficiently prolonged time. In other words, the best long-working Invar alloy in practice should be the one, in which the process of low-temperature annealing can provide the formation of microdomains of a required FeNi or Fe_3Ni composition. The alloy that corresponds to precisely such a composition is the one with a nickel content of 36 wt.%. With the deviation of the alloy composition on one side or the other, on the boundaries of growing microregions atoms of iron or nickel will be accumulated in surplus, which are not capable of forming one of the required phases; this will retard or change the kinetics of growth of ordered phases. Such a material will lose the qualitative characteristics of Invar sooner.

In the literature, it was repeatedly mentioned that the Invar effect is unstable and decreases substantially in the course of time. This is, apparently, due to the fact that, besides the possible appearance of defects in crystal structure, the prolonged annealings at low temperatures lead to an increase in the size of clusters and favor their transformation into the equilibrium FeNi-$L1_0$ phase.

There are data showing that after deformation or irradiation the Invar effect decreases. This, apparently, occurs because of the dissolution or, on the contrary, an easier nucleation of the Fe_3Ni phase on defects of crystal structure; in other words, as a result of the violation of the proportionality between the volume fractions of the FeNi and Fe_3Ni phases. The state of austenite passes into the region that does not correspond to Invar characteristics.

Thus, the 'Invar state' is metastable, whereas the contradictory experimental results available in the literature do not indicate the metastability of the FeNi-$L1_0$ and Fe_3Ni-$L1_2$ phases, but rather the kinetic dependence of the process of the precipitation of dispersed ordered phases coherently coupled with the matrix and between themselves on the temperature of quenching and subsequent annealing, on the degree of deformation, or on the irradiation dose.

6. Conclusions

Thus, based on the results of investigations conducted, the following conclusions can be made.

(1) The most reliable Fe–Ni phase diagram in its low-temperature part is the one published in Ref. [2], which is presented in Fig. 2b.

(2) For the first time, the formation of the equilibrium Fe_3Ni phase in an alloy of Invar composition Fe–32 at.% Ni has been experimentally realized and logically proven.

(3) It has been established that the equilibrium state of austenite at a temperature of 400 °C is a two-phase state: the $Fe_3Ni + \gamma$ phase enriched in nickel, owing to the detection of the discontinuous mechanism of the $\alpha \rightarrow \gamma$ phase transformation, which leads to the formation of equilibrium phases.

(4) It has been shown that at room temperature after slow cooling from 400 °C in the retained austenite there are domains of the ordered $L1_0$-FeNi phase, on the boundaries of which a network of dispersed precipitates of the Fe_3Ni phase is formed. The state that is equilibrium at room temperature is a two-phase state: $L1_0$-FeNi + $L1_2$-Fe_3Ni.

(5) The presence of the additional driving force in the $\alpha \rightarrow \gamma$ transformation or of an increased energy of boundaries in a deformed material [57] made it possible to establish that in the region of alloys with an Invar composition a precipitation occurs of the paramagnetic Fe_3Ni phase upon low-temperature annealing.

(6) The following assumption on the nature of the Invar effect was made: the proportional, interdependent growth of fcc ferromagnetically ordered FeNi clusters and of the ordered Fe_3Ni phase ensures a constant thermal expansion coefficient of the Fe–(30–40%) Ni alloys preliminarily subjected to quenching from high temperatures, upon subsequent low-temperature annealings.

Acknowledgments

The work was performed within the framework of the state assignment issued by Federal Agency of Scientific Organizations (FASO), Russia: theme 'Struktura' (Structure), state registration number 01201463331.

References

1. Hanson D, Hanson H E *J. Iron Steel Inst.* **102** 59 (1920)
2. Chamberod À, Laugier J, Penisson J M *J. Magn. Magn. Mater.* **10** 139 (1979)

3. Goman'kov V I et al., in *Strukturnyi Mekhanizm Fazovykh Prevrashchenii Metallov i Splavov* (Structural Mechanism of Phase Transformations in Metals and Alloys) (Eds O S Ivanov, R M Sofronova) (Moscow: Nauka, 1976) p. 153
4. Reuter K B, Williams D B, Goldstein J I *Met. Trans. A* **20** 711 (1989)
5. Yang J, Goldstein J I, in *Lunar and Planetary Science Conf. XXXIV, March 17–21, 2003*; http://www.lpi.usra.edu/meetings/lpsc2003/pdf/1156.pdf
6. Danilov S E, Arbusov V L, Kasantsev V A *Phys. Met. Metallogr.* **115** 126 (2014); *Fiz. Met. Metalloved.* **115** 134 (2014)
7. Petrova L A (Ed.) *Diagrammy Sostoyaniya Metallicheskikh Sistem, Opublikovannye v 1991 Godu* (Phase Diagrams of Metal Systems Published in 1991) Issue 36 (Moscow: VINITI, 1992) p. 127
8. Swartzendruber L J, Itkin V P, Alcock C B *J. Phase Equilibria* **12** 288 (1991)
9. Kybaschewski O *Iron-Binary Phase Diagrams* (Berlin: Springer-Verlag, 1982); Translated into Russian: *Diagrammy Sostoyaniya Dvoinykh Sistem na Osnove Zheleza. Spravochnik* (Ed. L M Bernshtein) (Moscow: Metallurgiya, 1985)
10. Silman G I *Metal Sci. Heat Treatment* **54** (3–4) 105 (2012); *MiTOM* (3) 3 (2012)
11. Heumann T, Karsten G *Arch. Eisenhüttenwesen* **34** 781 (1963)
12. Goman'kov V I, Sadchikov V V, Manaenkov S E *Materialovedenie* (9) 2 (2009)
13. Bando Y *J. Phys. Soc. Jpn.* **16** 2342 (1961)
14. Men'shikov A Z et al. *Phys. Met. Metallogr.* **34** (2) 78 (1972); *Fiz. Met. Metalloved.* **34** 309 (1972)
15. Aliev S S et al. *Metallofizika* **7** (5) 80 (1985)
16. Pauleve J et al. *J. Phys. Rad.* **23** 841 (1962)
17. Lysak L I, Artemyuk S A *Izv. Akad. Nauk SSSR Metally* (5) 170 (1973)
18. Krivoglaz M A, Smirnov A A *Teoriya Uporyadochivayushchikhsya Splavov* (Theory of Orderable Alloys) (Moscow: Fizmatlit, 1958)
19. Rizdvyanetskii D R, in *Metallofizika* Vol. 38 (Kiev: Naukova Dumka, 1971) p. 19
20. Chuang Y Y et al. *Metall. Trans. A* **17** 136 (1986)
21. Chuang Y Y, Hsieh K, Chang Y A A *Metall. Trans. A* **17** 1373 (1986)
22. Bolling G F, Richman R H *Acta. Met.* **18** 673 (1970)
23. Sagaradze V V, Zemtsova N D, Starthenko E I *Phys. Met. Metallogr.* **55** 99 (1983); *Fiz. Met. Metalloved.* **55** (1) 113 (1983)
24. Zambrzhitskii V I et al. *Dokl. Akad. Nauk SSSR* **230** 1330 (1976)
25. Ustinovshchikov Yu I *Phys. Usp.* **57** 670 (2014); *Usp. Fiz. Nauk* **184** 723 (2014)
26. Albertsen J F, Nielsen H P, Buchwald V F *Phys. Scripta* **27** 314 (1983)
27. Reuter K B, Williams D B, Goldstein J I *Meteoritics* **21** 493 (1986)
28. Reuter K B, Williams D B, Goldstein J I *Metall. Trans. A* **20** 719 (1989)
29. Yang C W, Williams D B, Goldstein J I *J. Phase Equilibria* **17** 522 (1996)
30. Cacciamani G at al. *Intermetallics* **18** 1148 (2010)
31. Mishin Y, Mehl M J, Papaconstantopoulos D A *Acta Mater.* **53** 4029 (2005)
32. Mohri T *J. Mater. Sci.* **50** 7705 (2015)
33. Warlimont H, Aubauer H *Z. Metallkunde* **64** 484 (1973)
34. Zemtsova N D, Sokolova A Yu *Phys. Met. Metallogr.* **82** (2) 186 (1996); *Fiz. Met. Metalloved.* **82** (2) 105 (1996)
35. Veeraraghavan V G et al. *J. Appl. Phys.* **47** 3768 (1976)
36. Xiong W et al. *Acta Mater.* **59** 521 (2011)
37. *The SGTE General Alloys Solutions Database, SSOL* Version 4.9f (Stockholm: Thermo-Calc AB, 2008)
38. Zemtsova N D *Tech. Phys.* **62** 731 (2017); *Zh. Tekh. Fiz.* **87** 710 (2017)
39. Zemtsova N D *Tech. Phys.* **62** 871 (2017); *Zh. Tekh. Fiz.* **87** 856 (2017)
40. Jana S, Wayman C M *Trans. Metall. Soc. AIME* **239** 1187 (1967)
41. Keßler H, Pitsch W *Arch. Eisenhüttenwesen* **38** 321 (1967)
42. Zemtsova N D, Malyshev K A, in *Strukturnyi Mekhanizm Fazovykh Prevrashchenii Metallov i Splavov* (Structural Mechanism of Phase Transformations in Metals and Alloys) (Eds O S Ivanov, R M Sofronova) (Moscow: Nauka, 1976) p. 138
43. Zemtsova N D, Starthenko E I *Phys. Met. Metallogr.* **50** 600 (1980); *Fiz. Met. Metalloved.* **50** 655 (1980)
44. Meny L, in *Microanalyse et microscopie Electronique a Balayage* (publiee sous la direction de F Maurice, L Meny, R Tixier) (Les Editions de Physique, France, 1978); Translated into Russian: in *Mikroanaliz i Rastrovaya Elektronnaya Mikroskopiya* (Eds F Maurice, L Meny, R Tixier) (Moscow: Metallurgiya, 1985)
45. Gleiter H, Chalmers B *High-angle Grain Boundaries* (Oxford: Pergamon Press, 1972); Translated into Russian: *Bol'sheuglovye Granitsy Zeren* (Moscow: Mir, 1975)
46. Sukhovarov V F *Preryvistoe Vydelenie Faz v Splavakh* (Discontinuous Precipitation of Phases in Alloys) (Novosibirsk: Nauka, Sib. Otdelenie, 1983)
47. Kaibyshev O A, Valiev R Z *Granitsy Zeren i Svoistva Metallov* (Grain Boundaries and Properties of Metals) (Moscow: Metallurgiya, 1987)
48. Kolobov Yu R *Diffuzionno-kontroliruemye Protsessy na Granitsakh Zeren i Plastichnost' Metallicheskikh Polikristallov* (Diffusion-Controlled Processes at Grain Boundaries and Plasticity of Metallic Polycrystals) (Novosibirsk: Nauka, 1998)
49. Ivanov M A, Glushchenko V I *Phys. Met. Metallogr.* **110** 415 (2010); *Fiz. Met. Metalloved.* **110** 435 (2010)
50. Zemtsova N D *Phys. Met. Metallogr.* **69** 136 (1990); *Fiz. Met. Metalloved.* (2) 140 (1990)
51. Zemtsova N D, Pereturina I A *Melallofizika* **14** (9) 7 (1992)
52. Glezer A M *Phys. Met. Metallogr.* **60** (2) 151 (1985); *Fiz. Met. Metalloved.* **60** 371 (1985)
53. Bondar' V I, Danil'chenko V Ye, Okhrimenko V A *Phys. Met. Metallogr.* **66** 146 (1988); *Fiz. Met. Metalloved.* **66** 157 (1988)
54. Abracham J K, Paskover J S *Trans. AIME* **245** 759 (1969)
55. Koval' Yu N, Kokorin V V *Fiz. Met. Metalloved.* **39** 1045 (1975)
56. Gun'ko L P, Kokorin V V *Dokl. Akad. Nauk SSSR* **240** 72 (1978)
57. Bitkulov I H at al. *Phys. Met. Metallogr.* **102** 91 (2006); *Fiz. Met. Metalloved.* **102** 99 (2006)
58. Freeman A J (Ed.) *Proc. of the Intern,Freeman, Symp. on "The Invar Problem" Nagoya, Japan, 4–6 September 1978*; *J. Magn. Magn. Mat.* **10** 109–316 (1979)
59. Wassermann E F *J. Magn. Magn. Mater.* **100** 346 (1991)
60. Ruban V *Phys. Rev. B* **71** 054402 (2005)
61. Mishin Y, Mehl M J, Papaconstantopoulos D D A *Acta Mater.* **53** 4029 (2005)
62. Ruban A V *Phys. Rev. B* **76** 014420 (2007)
63. Abrikosov I A *Phys. Rev. B* **76** 014434 (2007)
64. Mohri T *J. Mater. Sci.* **50** 7705 (2015)
65. Onoue M *J. Appl. Phys.* **117** 043912 (2015)
66. Mohn P, Schwarz K, Wagner D *Phys. Rev. B* **43** 3318 (1991)
67. Billard L, Chamberîd A *Solid State Commun.* **17** 113 (1975)
68. Voronchikhin L D, Zavadskii E A, Fakidov I G *Fiz. Met. Metalloved.* **22** 793 (1966)
69. Panin V E *Phys. Mesomech.* **1** 5 (1998); *Fiz. Mezomekh.* **1** 5 (1998)
70. Deryagin A I at al. *Phys. Met. Metallogr.* **89** 610 (2000); *Fiz. Met. Metalloved.* **89** (6) 82 (2000)
71. Zavalishin V A, Deryagin A I, Sagaradze V V *Phys. Met. Metallogr.* **75** 173 (1993); *Fiz. Met. Metalloved.* **75** 2 90 (1993)